Phonon-mediated spin-spin interaction: A general theory and application to diamond nitrogen vacancy centers

Jotaro J. Nakane ⬤, Kosuke Tahara ⬤, and Katsuhiro Kutsuki ⬤
Toyota Central R&D Labs., Inc., Nagakute, Aichi 480-1192, Japan

Ai Yamakage ⬤
Department of Physics, Nagoya University, Nagoya 464-8602, Japan

Interaction between spins forms diverse classes of magnetic materials. The interaction can be carried out not only by electrons and photons but also by phonons. We consider a general symmetry-allowed spin-phonon Hamiltonian in C_{3v} systems which consists of spins interacting with symmetric and antisymmetric lattice deformations. The derived model is used to calculate the phonon-mediated spin-spin interaction—the interaction is a quadrupole-quadrupole interaction. We first consider phonons in a homogeneous elastic medium, which leads to a spin-spin interaction with unphysical oscillations as a function of distance between the spins. We overcome this by extending the theory for lattice systems and confirm that the interaction strength decays as $1/r^3$. The effect of surface acoustic waves is also considered. The general theory is demonstrated for nitrogen vacancy centers in diamond as a prominent example. Furthermore, we provide an estimation of the magnitude of the spin-spin interaction and discuss the effect of the phonon-mediated spin-spin interaction on the energy level scheme of two interacting spins.

I. INTRODUCTION

Investigating the coupling between multiple spins is of central importance in condensed matter physics. The spin-spin interaction via electrons gives rise to the exchange coupling and the Ruderman-Kittel-Kasuya-Yosida (RKKY) interaction, and the interaction via photons gives rise to the magnetic dipole-dipole interaction. Coupling between spins may also be carried out by phonons. Phonon-induced spin-spin interaction, or the virtual phonon exchange, was first considered by Sugihara in 1959 [1] and later extended by other works, including in the context of the cooperative Jahn-Teller effect [2–6].

Phonon-induced spin-spin interaction could be significant in light of quantum technology involving spins in solids. One of the leading candidates of such spins is the negatively charged nitrogen vacancy (NV) color center in diamond, which is anticipated to become a spatially accurate multipurpose sensor that can measure electromagnetic fields, temperature, pressure, and rotation [7,8]. The quantum spin of NV centers is also expected to host quantum bits (qubits) for information processing [7,9–11]. A single NV center is well described by a spin-1 hard axis magnetic anisotropy Hamiltonian. In the case of multiple NV centers, magnetic dipole interaction [12] and magnon-mediated interaction [13,14] have been discussed. However, it is crucial to understand the full picture of the spin-spin interaction when one likes to utilize quantum spins for qubits and accurate sensors, so a theory describing the interactions between NV centers via phonons is also desired.

In this paper, we theoretically study the phonon-mediated spin-spin interaction in lattices. In Sec. II, we first prepare the general symmetry-allowed spin-phonon interaction in C_{3v} systems. In addition to the spin-strain coupling [15,16], we also consider the coupling of spins to the antisymmetric lattice deformation [17]. In Sec. III B, following previously used procedures, we first calculate the phonon-mediated spin-spin interaction in an elastic medium with a cutoff wave number in the integration (Debye approximation) [1,3], which we find gives rise to unphysical oscillations. Next, in Sec. III C, we employ a fcc crystal lattice to properly account for the Brillouin zone boundary and periodicity. In Sec. III D, the obtained spin-spin interaction is used to estimate the phonon-mediated spin-spin interaction coupling in diamond NV centers. We consider the energy level scheme of a two spin-1 system. The spin-spin interaction forms six energy states, three of which are spin degenerate. We discuss that under an applied magnetic field, six out of nine energy states show a 3θ dependence due to the spin-phonon interaction. Finally in Sec. III E, we calculate the surface acoustic wave mediated spin-spin interaction and compare the results.

II. SPIN-PHONON COUPLING

The general lowest-order spin-lattice interaction of a spin $\boldsymbol{S}$ embedded at $\boldsymbol{r}$ in a lattice interacting with the nearest-neighbor sites is written as

$$H = S_i(\boldsymbol{r})S_j(\boldsymbol{r})\sum_{\boldsymbol{d}} h_{ijk}(\boldsymbol{d})[u_k(\boldsymbol{r}+\boldsymbol{d}) - u_k(\boldsymbol{r})], \quad (1)$$

where $\boldsymbol{u}(\boldsymbol{r})$ is the displacement vector of the atom located at lattice point $\boldsymbol{r}$, h_{ijk} are the coupling constants, and the summation $\boldsymbol{d}$ is taken over the nearest-neighbor atoms. The order

of the spin operator must be even because of time-reversal symmetry, and S must be greater than 1/2 for there to be coupling with the lattice. The coupling constants are narrowed down by symmetry considerations.

Let us restrict ourselves to C_{3v} systems [18], with the threefold rotation axis in the z direction and the mirrors on the (xz) and equivalent planes. The spin coupling with the nearest-neighbor atoms must be totally symmetric with respect to the C_{3v} symmetry operations. Therefore, it is limited to the following form (see Appendix A for details):

$$H = S_z^2(\boldsymbol{r})[h_\parallel \tilde{q}_\parallel(\boldsymbol{r}) + h_\perp \tilde{q}_\perp(\boldsymbol{r})]$$
$$+ \sum_{i,j=1}^{2} \frac{h_{\mathrm{eg},ij}}{2} \boldsymbol{Q}_i(\boldsymbol{r}) \cdot \tilde{\boldsymbol{q}}_j(\boldsymbol{r}) + \sum_{i=1}^{2} D_i \boldsymbol{Q}_i(\boldsymbol{r}) \cdot \tilde{\boldsymbol{\omega}}(\boldsymbol{r}), \quad (2)$$

where we defined the spin vectors

$$\boldsymbol{Q}_1(\boldsymbol{r}) = (\{S^y(\boldsymbol{r}), S^z(\boldsymbol{r})\}, -\{S^z(\boldsymbol{r}), S^x(\boldsymbol{r})\}), \quad (3)$$

$$\boldsymbol{Q}_2(\boldsymbol{r}) = (\{S^x(\boldsymbol{r}), S^y(\boldsymbol{r})\}, [S^{x2}(\boldsymbol{r}) - S^{y2}(\boldsymbol{r})]), \quad (4)$$

with the anticommutator defined by $\{A, B\} = AB + BA$ and the atom displacement vectors

$$\tilde{q}_\parallel(\boldsymbol{r}) = \frac{1}{2\sqrt{2}\,a} \sum_{\boldsymbol{d}} \hat{d}_z u_z(\boldsymbol{r}+\boldsymbol{d}), \quad (5)$$

$$\tilde{q}_\perp(\boldsymbol{r}) = \frac{1}{2\sqrt{2}\,a} \sum_{\boldsymbol{d}} [\hat{d}_x u_x(\boldsymbol{r}+\boldsymbol{d}) + \hat{d}_y u_y(\boldsymbol{r}+\boldsymbol{d})], \quad (6)$$

$$\tilde{q}_1(\boldsymbol{r}) = \frac{1}{4\sqrt{2}\,a} \sum_{\boldsymbol{d}} [\hat{d}_y u_z(\boldsymbol{r}+\boldsymbol{d}) + \hat{d}_z u_y(\boldsymbol{r}+\boldsymbol{d}),$$
$$- \hat{d}_z u_x(\boldsymbol{r}+\boldsymbol{d}) - \hat{d}_x u_z(\boldsymbol{r}+\boldsymbol{d})], \quad (7)$$

$$\tilde{q}_2(\boldsymbol{r}) = \frac{1}{4\sqrt{2}\,a} \sum_{\boldsymbol{d}} [\hat{d}_x u_y(\boldsymbol{r}+\boldsymbol{d}) + \hat{d}_y u_x(\boldsymbol{r}+\boldsymbol{d}),$$
$$\hat{d}_x u_x(\boldsymbol{r}+\boldsymbol{d}) - \hat{d}_y u_y(\boldsymbol{r}+\boldsymbol{d})], \quad (8)$$

$$\tilde{\boldsymbol{\omega}}(\boldsymbol{r}) = \frac{1}{4\sqrt{2}\,a} \sum_{\boldsymbol{d}} [-\hat{d}_y u_z(\boldsymbol{r}+\boldsymbol{d}) + \hat{d}_z u_y(\boldsymbol{r}+\boldsymbol{d}),$$
$$- \hat{d}_z u_x(\boldsymbol{r}+\boldsymbol{d}) + \hat{d}_x u_z(\boldsymbol{r}+\boldsymbol{d})]. \quad (9)$$

$\hat{d}_i$ is the unit vector of the nearest-neighbor atoms, and the expression $\hat{d}_i u_j(\boldsymbol{r}+\boldsymbol{d})$ corresponds to the spatial derivative in the long wavelength limit as

$$\lim_{a \to 0} \sum_{\boldsymbol{d}} \frac{1}{2\sqrt{2}\,a} \hat{d}_i u_j(\boldsymbol{r}+\boldsymbol{d}) = \partial_i u_j(\boldsymbol{r}), \quad (10)$$

where we consider a fcc lattice with a lattice constant of the conventional cell a. The operators S_z^2, $\tilde{q}_\parallel$, and $\tilde{q}_\perp$ belong to the A_1 irreducible representation (irrep), while $\boldsymbol{Q}_1$, $\boldsymbol{Q}_2$, $\tilde{q}_1$, $\tilde{q}_2$, and $\tilde{\boldsymbol{\omega}}$ belong to the E_g irrep. Hence, they can be coupled with the same irrep, resulting in the Hamiltonian (2). $h_{\parallel, \perp, \mathrm{eg}}$ are the coupling constants between the spin and symmetric deformations $\tilde{q}$, and D_i are the coupling constants of the antisymmetric deformation $\tilde{\omega}$. In the long wavelength limit, coupling to $\tilde{q}$ reduces to the spin-strain coupling, and coupling to $\tilde{\omega}$ becomes the spin-rotational deformation coupling [17]. Note that D_1 coincides with the spin anisotropy energy D in the anisotropy Hamiltonian $H_S = DS_z^2$ and can be derived by

considering the tilting of the anisotropy axis due to rotational lattice deformations [17,19].

III. PHONON-MEDIATED SPIN-SPIN INTERACTION

A. Formalism

We consider two identical spins, $\boldsymbol{S}_1$ and $\boldsymbol{S}_2$, located at $\boldsymbol{r}_1$ and $\boldsymbol{r}_2$, respectively. The two spins are described by the Hamiltonians H_1 and H_2, respectively, and we evaluate their cross term in the second-order perturbation expansion. The thermodynamic potential of interest is given by

$$F_\omega = -\frac{1}{\beta} \int_0^\beta d\tau_1 d\tau_2 \langle T_\tau H_1(\tau_1) H_2(\tau_2) \rangle, \quad (11)$$

where β is the reciprocal of temperature, τ_1 and τ_2 are imaginary times, T_τ is the time-ordering operator, and $\langle \cdots \rangle$ is the grand-canonical ensemble average evaluated in the phonon Hamiltonian.

Let us introduce the phonon displacement as

$$\boldsymbol{u}(\boldsymbol{r}) = \sqrt{\frac{1}{2\rho V}} \sum_q \frac{\boldsymbol{e}_q e^{i\boldsymbol{q}\cdot\boldsymbol{r}}}{\sqrt{\omega_q}} a_q + \mathrm{H.c.}, \quad (12)$$

where ω_q, $\boldsymbol{e}_q$, and a_q are, respectively, the frequency, polarization vector, and annihilation operator of the phonon with $q = \{\boldsymbol{q}, \lambda\}$ ($\boldsymbol{q}$ is the wave vector and λ is the polarization). V is the volume of the lattice, and ρ is the mass density.

B. Debye approximation

In this section, we outline the calculation for the phonon-mediated spin-spin interaction by considering only the D_1 term in Eq. (2) in the long wavelength limit. The D_1 term in the long wavelength limit is given by

$$H_\omega = D(\varepsilon_{zx-}\{S_z, S_x\} - \varepsilon_{yz-}\{S_y, S_z\}), \quad (13)$$

where $\varepsilon_{ij-} = (\partial_i u_j - \partial_j u_i)/2$ is the rotational deformation evaluated at the spin site.

For simplicity, we first adopt the dispersion and polarization vectors for an isotropic elastic medium. The polarization vector is taken to be real and orthonormal, $\boldsymbol{e}_{q1} \times \boldsymbol{e}_{q2} = \boldsymbol{e}_{q3}$, with the longitudinal mode parallel to the wave vector, $\boldsymbol{e}_{q3} \parallel \boldsymbol{q}$. The energy dispersion consists of two degenerate transverse modes $\omega_{q1} = \omega_{q2} \equiv \omega_{q\perp}$ and one longitudinal mode ω_{q3}. Phonon dispersion is taken to be linear, with $\omega_{q\perp} = c_\perp |\boldsymbol{q}|$ and $\omega_{q3} = c_\parallel |\boldsymbol{q}|$. The two spins are assumed to be located along the z axis as $\boldsymbol{r}_1 - \boldsymbol{r}_2 = r_z \hat{z}$. Then, the spin-spin interaction can be evaluated by the summation

$$F_\omega = \frac{D^2}{4\rho V} \sum_q \frac{\cos(q_z r_z)}{-\omega_{q\perp}^2} [(\hat{y} \times \boldsymbol{q})^2 \{S_1^z, S_1^x\}\{S_2^z, S_2^x\}$$
$$+ (\hat{x} \times \boldsymbol{q})^2 \{S_1^y, S_1^z\}\{S_2^y, S_2^z\}], \quad (14)$$

where we dropped the term with the odd integrand proportional to $(\hat{y} \times \boldsymbol{q}) \cdot (\hat{x} \times \boldsymbol{q})$. Considering a spherical domain of integration, $|\boldsymbol{q}| < q_D$, with q_D being the Debye cutoff wave number $q_D \sim (4\pi^2 \rho_i)^{1/3}$ (ρ_i is the lattice point density), the spin-spin interaction takes the form

$$F_\omega = J(r_z)(\{S_1^z, S_1^x\}\{S_2^z, S_2^x\} + \{S_1^y, S_1^z\}\{S_2^y, S_2^z\}), \quad (15)$$
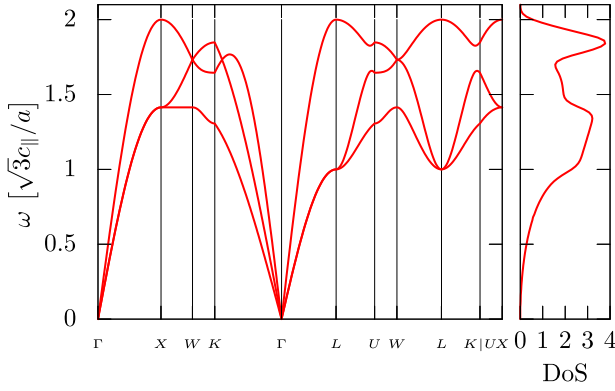
FIG. 1. Dispersion relation and density of states (DOS) of the fcc lattice phonon.

and the coupling constant is given by

$$
J(r_z) = \frac{D^2}{8\pi^2 \rho c_\perp^2} \frac{r_z q_D \cos(r_z q_D) - 2\sin(r_z q_D) + \mathrm{Si}(r_z q_D)}{r_z^3},
\tag{16}
$$

where $\mathrm{Si}(x) \equiv \int_0^x dt\ \sin(t)/t$ is the sine integral function. The interaction is an even function of r_z (as it should be since the interaction must be invariant under the exchange of S_1 and S_2). Not unlike in the RKKY interaction, we have a long-range oscillatory spin-spin interaction with wavelength $(q_D)^{-1}$. It appears that the most long-range interaction is of order r^{-2}, which would be remarkable since other long-range interactions, such as the magnetic dipole-dipole interaction, are of order r^{-3}. Like in Ref. [1], we have two oscillating terms of the forms $\cos(r_z q_D)$ and $\sin(r_z q_D)$ and one term proportional to r^{-3} without much oscillation for large r/a. Sugihara's procedure of deeming the oscillating terms unimportant, in which case $J(r_z)$ is always positive, is not well justified because the trigonometric functions could be of order unity at the lattice points. Also, the explicit dependence on the Debye wave number suggests that the shape of the Brillouin zone could be important—we must abandon the Debye approximation.

C. fcc crystal

Let us consider a fcc crystal with only the nearest-neighbor interaction present. The eigenvalue equation for lattice vibrations in the conventional cell frame is given by

$$
\frac{\omega^2}{3c_\parallel^2} \boldsymbol{e} = D_{\boldsymbol{q}} \boldsymbol{e},
\tag{17}
$$

where the matrix element of $D_{\boldsymbol{q}}$ is

$$
D_{\boldsymbol{q}}^{ij} = \begin{cases} 2 - \cos\left(\frac{q_i a}{2}\right) \sum_{m \neq i} \cos\left(\frac{q_m a}{2}\right) & \text{if } i = j, \\ \sin\left(\frac{q_i a}{2}\right) \sin\left(\frac{q_j a}{2}\right) & \text{if } i \neq j. \end{cases}
\tag{18}
$$

The lattice constant, which is the side length of the conventional cell, is taken to be 1, and $c_\parallel$ is the longitudinal sound velocity in the [111] direction. The obtained dispersion relation and density of states are shown in Fig. 1.

In the fcc lattice, the variation in the lattice displacement must be written in wave number space as

$$
\sum_{\boldsymbol{d}} \frac{1}{2\sqrt{2}\,a} \hat{d}_i u_j = i \frac{v_i}{a} u_j,
\tag{19}
$$

where the vector v_i is given by

$$
v_i = \sin\left(\frac{q_i a}{2}\right) \sum_{j \neq i} \cos\left(\frac{q_j a}{2}\right),
\tag{20}
$$

which coincides with Eq. (10) in the long wavelength limit. We are now equipped to calculate the spin-spin interaction in fcc crystals.

Let us write the contribution from phonons as

$$
-\frac{1}{\beta} \int d\tau_1 d\tau_2 \langle T_\tau \varepsilon_{ij\pm}(\boldsymbol{r}_1, \tau_1) \varepsilon_{kl\pm'}(\boldsymbol{r}_2, \tau_2) \rangle
$$
$$
\equiv \langle \varepsilon_{ij\pm}(\boldsymbol{r}_1) \varepsilon_{kl\pm'}(\boldsymbol{r}_2) \rangle_{\mathrm{ph}},
\tag{21}
$$

where $\varepsilon_{ij\pm}(\boldsymbol{r}) = \sum_{\boldsymbol{d}} [\hat{d}_i u_j(\boldsymbol{r}) \pm \hat{d}_j u_i(\boldsymbol{r})]/(4\sqrt{2}\,a)$. They satisfy the properties $\langle \varepsilon_{ij\pm}(\boldsymbol{r}_1) \varepsilon_{kl\pm'}(\boldsymbol{r}_2) \rangle_{\mathrm{ph}} = \langle \varepsilon_{ij\pm}(\boldsymbol{r}_2) \varepsilon_{kl\pm'}(\boldsymbol{r}_1) \rangle_{\mathrm{ph}}$ and $\langle \varepsilon_{ij\pm}(\boldsymbol{r}_1) \varepsilon_{kl\pm'}(\boldsymbol{r}_2) \rangle_{\mathrm{ph}} = \langle \varepsilon_{kl\pm'}(\boldsymbol{r}_1) \varepsilon_{ij\pm}(\boldsymbol{r}_2) \rangle_{\mathrm{ph}}$. The tensors ε_{ij+} and ε_{ij-} become the strain and rotational deformation tensors, $\varepsilon_{ij\pm} \to (\partial_i u_j \pm \partial_j u_i)/2$, respectively, in the long wavelength limit. Note that the position $\boldsymbol{r}$ of the spin is discrete and must be on the fcc lattice sites. We will suppress the $\boldsymbol{r}$ dependence hereafter.

Let us again consider only the D_1 term in Eq. (2) to illustrate the calculation. The spin-spin interactions for $\boldsymbol{r}_1 - \boldsymbol{r}_2 = r_z \hat{z}$ can be written as

$$
F_\omega = J(r_z)\left(\{S_1^z, S_1^x\}\{S_2^z, S_2^x\} + \{S_1^y, S_1^z\}\{S_2^y, S_2^z\} \right),
\tag{22}
$$

where

$$
J(r_z) = D^2 \langle \varepsilon_{yz-}(\boldsymbol{r}_1) \varepsilon_{yz-}(\boldsymbol{r}_2) \rangle_{\mathrm{ph}}.
\tag{23}
$$

Note that $\langle \varepsilon_{yz-} \varepsilon_{yz-} \rangle_{\mathrm{ph}} = \langle \varepsilon_{zx-} \varepsilon_{zx-} \rangle_{\mathrm{ph}}$ and $\langle \varepsilon_{yz-} \varepsilon_{zx-} \rangle_{\mathrm{ph}} = 0$ by symmetry. Using the Newton-Cotes formulas for
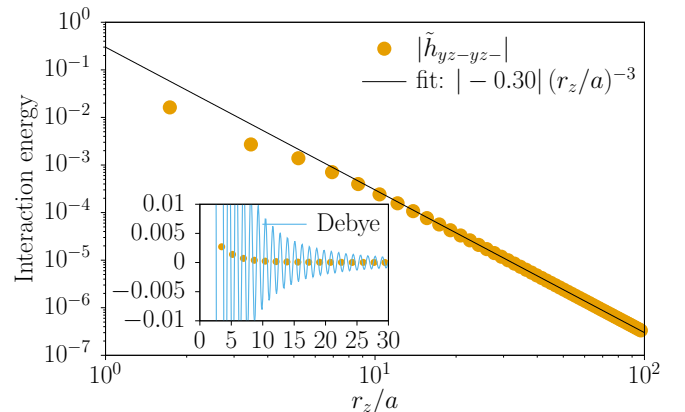

FIG. 2. Plot of the numerical calculation for $\tilde{h}_{yz-yz-} \equiv 3\rho a^3 c_\parallel^2 \langle \varepsilon_{yz-}(\boldsymbol{r}_1) \varepsilon_{yz-}(\boldsymbol{r}_2) \rangle_{\mathrm{ph}}$ as a function of distance in log-log scale (orange) and a line of best fit. We see that the distance dependence is of the form r_z^{-3}. Since the current model is based on the spin-strain coupling, the theory is applicable only to distances $\gg a$, and the fitting is done for points greater than $20a$. The inset plots $\tilde{h}_{yz-yz-}$ evaluated in the Debye approximation [Eq. (16)], where we have $q_D a = (4\pi)^{2/3}$ and $c_\parallel \simeq 2c_\perp$.

TABLE I. All independent phonon-induced spin-spin coupling parameters. The dimensionless parameters are defined as $\tilde{h}_{ij\pm kl\pm'} = 3\rho a^3 c_\parallel^2 \langle \varepsilon_{ij\pm}\varepsilon_{kl\pm'}\rangle_{\rm ph}$. Parameters have a distance dependence of r_z^{-3}. Numerical fitting was done for spins separated by distance $>20a$.

Parameter	Value [in units of $(r_z/a)^{-3}$]
$\tilde{h}_{zz+zz+}$	2.0360
$\tilde{h}_{zz+xx+}$	-0.5254
$\tilde{h}_{xx+xx+}$	-0.03557
$\tilde{h}_{xx+yy+}$	0.23117
$\tilde{h}_{xx+zx+}$	-0.16449
$\tilde{h}_{xx+zx-}$	0.26372
$\tilde{h}_{zx+zx+}$	-0.8239
$\tilde{h}_{zx+zx-}$	1.0944
$\tilde{h}_{zx-zx-}$	-0.2985

numeric integration, we plot the nondimensionalized $\langle \varepsilon_{yz-}(\boldsymbol{r}_1)\varepsilon_{yz-}(\boldsymbol{r}_2)\rangle_{\rm ph}$ in Fig. 2, together with a line of best fit. We see that $\langle \varepsilon_{yz-}(\boldsymbol{r}_1)\varepsilon_{yz-}(\boldsymbol{r}_2)\rangle_{\rm ph}$ is a long-range interaction of the form $1/r_z^3$. We also observe that the oscillatory behavior that was present in Eq. (16) is gone (see inset in Fig. 2). This is because we evaluate $\langle \varepsilon_{yz-}(\boldsymbol{r}_1)\varepsilon_{yz-}(\boldsymbol{r}_2)\rangle_{\rm ph}$ only on the lattice points; unphysical oscillation with the wavelength dependent on the Brillouin zone boundary appears between the lattice points. The $1/r_z^2$ term in Eq. (16) vanishes, and the sign of the analytical result differs from the numerical calculation if one chooses to follow Sugihara's procedure and consider only the sine integral term in Eq. (16) (see Table I for all fitting constants). This can be understood if one requires Eq. (16) to be invariant under translation by a reciprocal lattice vector, $q_D \to q_D + G$. The only term that can fulfill this requirement is the second term, which is inversely proportional to r^3 and may be positive as well as negative, in accordance with our numeric result. The integrand of $\langle \varepsilon_{yz-}(\boldsymbol{r}_1)\varepsilon_{yz-}(\boldsymbol{r}_2)\rangle_{\rm ph}$ is plotted in Fig. 3 as a function of wave number from Γ to L for some values of r_z.

Let us now consider the spin-spin interaction in a general C_{3v} system [Eq. (2)] due to phonons described by Eq. (17),

$$F = J_{\rm a1}S_z^2(\boldsymbol{r}_1)S_z^2(\boldsymbol{r}_2) + \sum_{i,j}^2 J_{{\rm eg},ij}\boldsymbol{Q}_i(\boldsymbol{r}_1)\cdot\boldsymbol{Q}_j(\boldsymbol{r}_2) \quad (24)$$
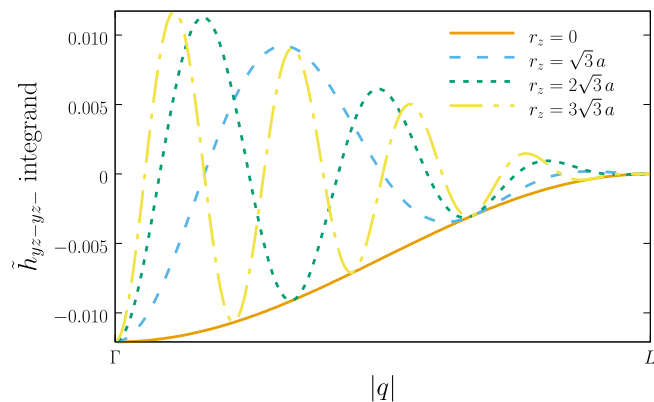

FIG. 3. Nondimensionalized integrand of $\langle \varepsilon_{yz-}(\boldsymbol{r}_1)\varepsilon_{yz-}(\boldsymbol{r}_2)\rangle_{\rm ph}$ as a function of wave number, plotted from Γ to L. The number of nodes increases as the distance between the spins increases.

for $\boldsymbol{r}_1 - \boldsymbol{r}_2 = r_z\boldsymbol{e}_z$, where $J_{\rm a1,eg}$ are effective spin-spin coupling constants due to phonons and $J_{{\rm eg},12} = J_{{\rm eg},21}$ follows from inversion symmetry. The above equation is the only form allowed by symmetry. $\boldsymbol{Q}_i$ belongs to the E irreducible representation of C_{3v} (see Appendix A); hence, $\boldsymbol{Q}_i \cdot \boldsymbol{Q}_j$ is totally symmetric. The coefficients are given in terms of the microscopic coupling constants as

$$J_{\rm a1} = \langle A^z(\boldsymbol{r}_1)A^z(\boldsymbol{r}_2)\rangle_{\rm ph}, \quad (25)$$

$$J_{{\rm eg},ij} = \langle \boldsymbol{A}_i(\boldsymbol{r}_1)\cdot\boldsymbol{A}_j(\boldsymbol{r}_2)\rangle_{\rm ph}, \quad (26)$$

where A^z and $\boldsymbol{A}_i$ are defined by quadratic moments of the phonon field, which can be coupled with the spins as

$$A^z = h_\parallel\tilde{q}_\parallel + h_\perp\tilde{q}_\perp, \quad (27)$$

$$\boldsymbol{A}_i = D_i\tilde{\boldsymbol{\omega}} + \sum_{j=1}^2 \frac{h_{{\rm eg},ij}}{2}\tilde{\boldsymbol{q}}_j. \quad (28)$$

In terms of these moments, the spin-lattice Hamiltonian (2) reduces to

$$H = S^{z2}A^z + \sum_{i=1}^2 \boldsymbol{Q}_i \cdot \boldsymbol{A}_i. \quad (29)$$

From numerical fitting, we obtain the mutually independent values in Table I. We see that all parameters have a distance dependence of r_z^{-3}.

D. Diamond NV centers

Finally, let us focus on NV centers in diamond. Since a NV center has C_{3v} symmetry, the spin-phonon coupling is given by Eq. (2). The symmetric coupling constants, $h_\parallel$, $h_\perp$, and $h_{{\rm eg},ij}$, for NV centers in diamond are substituted by the spin-strain coupling found in Refs. [15,16], and the antisymmetric coupling constant is given by $D_1 = 2.87$ GHz. The term with D_2 is dropped because it stems from a higher-order magnetic anisotropy [20]. Here, we use the spin-strain coupling constants obtained from first-principles calculations by Udvarhelyi *et al.* [15], $h_\parallel = 2.3 \pm 0.2$ GHz, $h_\perp = -6.42 \pm 0.09$ GHz, $h_{{\rm eg},12} = -2.60 \pm 0.08$ GHz, $h_{{\rm eg},11} = -2.83 \pm 0.07$ GHz, $h_{{\rm eg},22} = 5.7 \pm 0.2$ GHz, and $h_{{\rm eg},21} = 19.66 \pm 0.09$ GHz. Other parameters are given by $c_\parallel = 19\,039$ m s^{-1} [21], $a = 0.357$ nm [22], and $\rho = 3520$ kg m^{-3} [23]. Note that our approximation is applicable only to distances much greater than a because the parameters are based on uniform spin-strain coupling. Also, optical phonons are dropped. We can now estimate the spin-spin coupling via phonons in diamond NV centers:

$$J_{\rm a1} = 220 \pm 10 \quad (r_z/a)^{-3} \text{ Hz}, \quad (30)$$

$$J_{{\rm eg},22} = -272 \pm 2 \quad (r_z/a)^{-3} \text{ Hz}, \quad (31)$$

$$J_{{\rm eg},11} = -41 \pm 1 \quad (r_z/a)^{-3} \text{ Hz}, \quad (32)$$

$$J_{{\rm eg},12} = 144 \pm 1 \quad (r_z/a)^{-3} \text{ Hz}. \quad (33)$$

A positive $J_{\rm a1}$ prefers smaller S_z for both spins, unless one spin is orthogonal to z; in this case the other spin does not change energy regardless of its direction. A negative $J_{{\rm eg},22}$

implies that the two spins prefer to be parallel or antiparallel to each other in the xy plane. A negative $J_{eg,11}$ prefers both spins to be parallel or antiparallel to each other while being tilted from the z axis by $\pi/4$ or $3\pi/4$. Finally, a nonzero $J_{eg,12}$ is reflective of the threefold rotational symmetry, and a positive $J_{eg,12}$ means that the two spins prefer to be parallel or antiparallel to each other, with a tilt from the z axis by $\pi/3$ or $2\pi/3$ and azimuthal angle $2\pi n/3$ or $(2n+1)\pi/3$, $n \in \{0, 1, 2\}$, respectively.

The interaction also gives rise to attractive and repulsive interactions between the color centers. Unlike point defects without spin which have a fixed sign of interaction [24,25], interaction between color centers can be both attractive and repulsive, depending on the spin orientation. For example, when both spins between the spins point in the z direction, the two color centers repel each other, and when the two spins point in the x direction, the two spins attract each other.

1. Comparison with dipole-dipole interaction

Let us compare the magnitude of the phonon-induced spin-spin interaction with magnetic dipole-dipole interaction. Magnetic dipole-dipole interaction is given by

$$H_{\text{dip}-\text{dip}} = -\frac{\mu_0 \gamma^2 \hbar^2}{4\pi |r|^3} [3(\boldsymbol{S}_1 \cdot \hat{\boldsymbol{r}})(\boldsymbol{S}_2 \cdot \hat{\boldsymbol{r}}) - \boldsymbol{S}_1 \cdot \boldsymbol{S}_2], \quad (34)$$

where μ_0 is the vacuum permeability, $\mu_0 = 2\alpha h/(e^2 c)$ (α is the fine-structure constant), and $\gamma = g\mu_B/\hbar$ is the gyromagnetic ratio, with $\mu_B = e\hbar/(2m)$ being the Bohr magneton. Then, the magnetic dipole-dipole energy can be estimated as

$$H_{\text{dip}-\text{dip}} \simeq J_{\text{dip}}[3(\boldsymbol{S}_1 \cdot \hat{\boldsymbol{r}})(\boldsymbol{S}_2 \cdot \hat{\boldsymbol{r}}) - \boldsymbol{S}_1 \cdot \boldsymbol{S}_2], \quad (35)$$

with $J_{\text{dip}} \simeq -1 \times 10^9 \, (r_z/a)^{-3}$ Hz. Therefore, since both phonon-mediated spin-spin interaction and magnetic dipole-dipole interactions have a distance dependence of $1/r_z^3$, spin-spin interaction in diamond is dominated by the magnetic dipole-dipole interaction. Nevertheless, it is the largest quadrupole-quadrupole interaction. Since the phonon-mediated spin-spin interaction coupling constant $J \propto (D \text{ or } h_{\parallel, \perp, eg})^2 \rho^{-1} c^{-2}$, where c is the elastic wave velocity, one can expect large phonon-mediated spin-spin interactions in materials with large spin-phonon interaction, low elastic wave velocity, and low mass density.

2. Energy level scheme

Finally, let us discuss the energy level scheme of the two spins. The eigenenergies of the two spins are

$$\omega_{E_u} = D + J_{\text{dip}} - J_{\text{eg}11}, \quad (36)$$

$$\omega_{E_g}' = \frac{1}{2}\Big[3D + J_{\text{dip}} + J_{\text{a}1} + J_{\text{eg}11}$$
$$- \sqrt{(D + 3J_{\text{dip}} + J_{\text{a}1} - J_{\text{eg}11})^2 + 16J_{\text{eg}12}^2}\Big], \quad (37)$$

$$\omega_{E_g} = \frac{1}{2}\Big[3D + J_{\text{dip}} + J_{\text{a}1} + J_{\text{eg}11}$$
$$+ \sqrt{(D + 3J_{\text{dip}} + J_{\text{a}1} - J_{\text{eg}11})^2 + 16J_{\text{eg}12}^2}\Big], \quad (38)$$

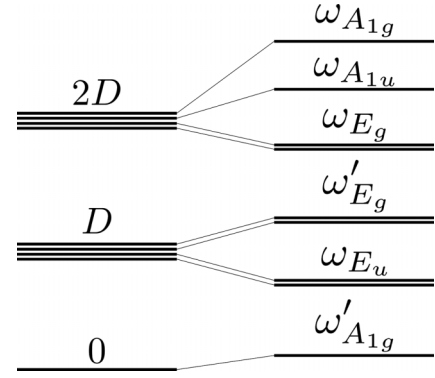$$\omega_{A_{1u}} = 2D + J_{\text{a}1} - 2(J_{\text{dip}} + J_{\text{eg}22}), \quad (39)$$

FIG. 4. There are nine energy levels for a two spin-1 system. On the left are the energy levels when only magnetic anisotropy energy D is present. In this case, the energies $2D$ and D are fourfold degenerate, and the ground state energy is nondegenerate. With the introduction of the magnetic dipole energy and phonon-induced spin-spin interaction, the fourfold-degenerate energy levels split into three twofold-degenerate levels and two nondegenerate levels.

$$\omega_{A_{1g}}' = D - J_{\text{dip}} + \frac{1}{2}J_{\text{a}1} + J_{\text{eg}22}$$
$$- \sqrt{\left(D - J_{\text{dip}} + \tfrac{1}{2}J_{\text{a}1} + J_{\text{eg}22}\right)^2 + 2(J_{\text{dip}} + J_{\text{eg}11})^2}, \quad (40)$$

$$\omega_{A_{1g}} = D - J_{\text{dip}} + \frac{1}{2}J_{\text{a}1} + J_{\text{eg}22}$$
$$+ \sqrt{\left(D - J_{\text{dip}} + \tfrac{1}{2}J_{\text{a}1} + J_{\text{eg}22}\right)^2 + 2(J_{\text{dip}} + J_{\text{eg}11})^2}, \quad (41)$$

where ω_{E_u}, ω_{E_g}', and ω_{E_g} are twofold degenerate and $\omega_{A_{1u}}$, $\omega_{A_{1g}}'$, and $\omega_{A_{1g}}$ are not (see Fig. 4). Under an applied magnetic field in the z direction, all twofold degeneracies are resolved, while the nondegenerate energy levels ($\omega_{A_{1u}}$, $\omega_{A_{1g}}'$ and $\omega_{A_{1g}}$) are immune.

By symmetry arguments, one can show that under an applied magnetic field of the form $\boldsymbol{H} = (H_\perp \cos\theta, \, H_\perp \sin\theta, \, H_z)$, The six energy states corresponding to ω_{E_g}', ω_{E_g}, $\omega_{A_{1g}}'$, and $\omega_{A_{1g}}$ states show a 3θ dependence because of the coupling constant $J_{\text{eg}12}$, while the remaining three states corresponding to $\omega_{A_{1u}}$ and ω_{E_u} are not dependent on θ.

E. Surface acoustic wave mediated spin-spin interaction

So far, we have investigated phonons in three-dimensional bulk materials without considering surface effects. However, realistic experimental setups often have color centers embedded near the surface of the diamond substrate [26–28]. Therefore, let us consider the surface acoustic wave mediated spin-spin interaction.

The Rayleigh waves are quantized as

$$\boldsymbol{u}^{\text{R}}(\boldsymbol{r}) = \sqrt{\frac{1}{2\rho V}} \sum_{\boldsymbol{q}_\perp} \frac{\boldsymbol{e}_{\boldsymbol{q}_\perp}^{\text{R}} e^{i\boldsymbol{q}_\perp \cdot \boldsymbol{r}}}{\sqrt{\omega_{\boldsymbol{q}_\perp}^{\text{R}}}} a_{\boldsymbol{q}_\perp}^{\text{R}} + \text{H.c.}, \quad (42)$$

where $\omega_{\boldsymbol{q}_\perp}^{\text{R}}$, $\boldsymbol{e}_{\boldsymbol{q}_\perp}^{\text{R}}$, and $a_{\boldsymbol{q}_\perp}^{\text{R}}$ are the frequency, polarization vector, and annihilation operator of the Rayleigh wave, respectively.

We assume the medium is located in half-space $x < 0$, and $\boldsymbol{q}_\perp = (q_y, q_z)$ is the wave number parallel to the surface [29]. Note that the inner product is normalized as $\int_{-\infty}^0 dx\,(e_{\boldsymbol{q}_\perp}^{\mathrm{R}})^* \cdot e_{\boldsymbol{q}_\perp}^{\mathrm{R}} = 1$, where

$$
e_{\boldsymbol{q}_\perp}^{\mathrm{R}x} = \gamma \sqrt{\frac{q_\perp}{K_\sigma}}\left[e^{\kappa_\ell x} - \frac{2}{1+\eta^2}e^{\kappa_t x}\right],
$$

$$
e_{\boldsymbol{q}_\perp}^{\mathrm{R}y} = i\frac{q_y}{q_\perp}\sqrt{\frac{q_\perp}{K_\sigma}}\left[e^{\kappa_\ell x} - \frac{2\eta\gamma}{1+\eta^2}e^{\kappa_t x}\right],
$$

$$
e_{\boldsymbol{q}_\perp}^{\mathrm{R}z} = i\frac{q_z}{q_\perp}\sqrt{\frac{q_\perp}{K_\sigma}}\left[e^{\kappa_\ell x} - \frac{2\eta\gamma}{1+\eta^2}e^{\kappa_t x}\right], \tag{43}
$$

$|\boldsymbol{q}_\perp| = q_\perp$, and the phase is chosen so that $(e_{\boldsymbol{q}_\perp}^{\mathrm{R}})^* = e_{-\boldsymbol{q}_\perp}^{\mathrm{R}}$. The inverse penetration depths of the surface acoustic wave are given by

$$
\kappa_\ell = \gamma q_\perp = \sqrt{q_\perp^2 - \left(\omega_{\boldsymbol{q}_\perp}^{\mathrm{R}}/c_\parallel\right)^2},
$$

$$
\kappa_t = \eta q_\perp = \sqrt{q_\perp^2 - \left(\omega_{\boldsymbol{q}_\perp}^{\mathrm{R}}/c_\perp\right)^2} \tag{44}
$$

and $c_\parallel$ and $c_\perp$ are the bulk longitudinal and transverse wave velocities, respectively. The normalization constant K_σ is given by

$$
K_\sigma = \frac{(\gamma - \eta)(\gamma - \eta + 2\eta^2\gamma)}{2\eta^2\gamma}. \tag{45}
$$

The dispersion relation of the surface acoustic wave can be obtained from the relation [30]

$$
\left(q_\perp^2 + \kappa_t^2\right)^2 = 4q_\perp^2\kappa_t\kappa_\ell, \tag{46}
$$

which is given by $\omega_{\boldsymbol{q}_\perp}^{\mathrm{R}} = v^{\mathrm{R}}q_\perp$. Following the procedures in Secs. III A and III B and assuming S_1 and S_2 are placed at $(r_x, 0, 0)$ and $(r_x, 0, r_z)$, respectively, with $r_x < 0$, we have a surface acoustic wave mediated spin-spin interaction given by

$$
-\frac{1}{\beta}\int_0^\beta d\tau_1 d\tau_2 \langle T_\tau H_1(\tau_1)H_2(\tau_2)\rangle_{\mathrm{R}} \tag{47}
$$

$$
\begin{aligned}
= \; & [S_z(\boldsymbol{r}_1)]^2[S_z(\boldsymbol{r}_2)]^2 J_{zz}(\boldsymbol{r}_1 - \boldsymbol{r}_2) \\
& + \left\{[S_z(\boldsymbol{r}_1)]^2 Q_1^2(\boldsymbol{r}_2)J_{zQ_1^2}(\boldsymbol{r}_1 - \boldsymbol{r}_2) + \boldsymbol{r}_1 \leftrightarrow \boldsymbol{r}_2\right\} \\
& + \left\{[S_z(\boldsymbol{r}_1)]^2 Q_2^2(\boldsymbol{r}_2)J_{zQ_2^2}(\boldsymbol{r}_1 - \boldsymbol{r}_2) + \boldsymbol{r}_1 \leftrightarrow \boldsymbol{r}_2\right\} \\
& + Q_1^2(\boldsymbol{r}_1)Q_1^2(\boldsymbol{r}_2)J_{Q_1^2 Q_1^2}(\boldsymbol{r}_1 - \boldsymbol{r}_2) \\
& + \left\{Q_1^2(\boldsymbol{r}_1)Q_2^2(\boldsymbol{r}_2)J_{Q_1^2 Q_2^2}(\boldsymbol{r}_1 - \boldsymbol{r}_2) + \boldsymbol{r}_1 \leftrightarrow \boldsymbol{r}_2\right\} \\
& + Q_2^2(\boldsymbol{r}_1)Q_2^2(\boldsymbol{r}_2)J_{Q_2^2 Q_2^2}(\boldsymbol{r}_1 - \boldsymbol{r}_2) \\
& + Q_1^1(\boldsymbol{r}_1)Q_1^1(\boldsymbol{r}_2)J_{Q_1^1 Q_1^1}(\boldsymbol{r}_1 - \boldsymbol{r}_2) \\
& + \left\{Q_1^1(\boldsymbol{r}_1)Q_2^1(\boldsymbol{r}_2)J_{Q_1^1 Q_2^1}(\boldsymbol{r}_1 - \boldsymbol{r}_2) + \boldsymbol{r}_1 \leftrightarrow \boldsymbol{r}_2\right\} \\
& + Q_2^1(\boldsymbol{r}_1)Q_2^1(\boldsymbol{r}_2)J_{Q_2^1 Q_2^1}(\boldsymbol{r}_1 - \boldsymbol{r}_2), \tag{48}
\end{aligned}
$$

where the average is now taken in the surface acoustic wave phonon Hamiltonian. More terms appear compared to the bulk result because the system now has only mirror symmetry in the y direction. Therefore, the only requirement by symmetry is that Q_i^1 does not have any cross terms with Q_j^2 and S_z^2 for any i, j. The coefficients in the shallow limit $|x| \ll |\boldsymbol{r}_1 - \boldsymbol{r}_2|$ are given in Appendix B.

TABLE II. Numerical values of Eqs. (B1)–(B9) evaluated using parameters from Refs. [15,21–23,31].

Parameter	Value [in units of $(r_z/a)^{-3}$Hz]
$J_{zz}(r_z)$	-1.99×10^2
$J_{zQ_1^2}(r_z)$	$1.82 \times 10^1 - 3.80 \times 10^1\,\mathrm{sgn}(r_z)$
$J_{zQ_2^2}(r_z)$	-3.99×10^1
$J_{Q_1^2 Q_1^2}(r_z)$	7.65×10^1
$J_{Q_1^2 Q_2^2}(r_z)$	$3.36 + 1.24 \times 10^1\,\mathrm{sgn}(r_z)$
$J_{Q_2^2 Q_2^2}(r_z)$	-7.37
$J_{Q_1^1 Q_1^1}(r_z)$	4.62
$J_{Q_1^1 Q_2^1}(r_z)$	-3.21×10^1
$J_{Q_2^1 Q_2^1}(r_z)$	2.23×10^2

Because of the exponential decay of the integrand, the integration converges without a Debye cutoff. The Debye cutoff is extended to infinity, which is justified for $|\gamma x/a| \gg 1$ and $|\eta x/a| \gg 1$, where a is the lattice constant.

The surface acoustic wave mediated spin-spin interaction in the shallow limit is proportional to $1/r_z^3$, similar to the bulk phonon-mediated spin-spin interaction. Poisson's ratio σ for diamond is around 0.0691 [31]. Thus, from the relation $\frac{c_\perp}{c_\parallel} = \sqrt{\frac{1-2\sigma}{2-2\sigma}}$, we have $\eta = 0.46115$ and $\gamma = 0.79722$. With the longitudinal sound velocity in diamond $c_\parallel = 19039\,\mathrm{m\,s^{-1}}$ [21], we obtain the velocity of the Rayleigh wave $v_{\mathrm{R}} = 11494\,\mathrm{m\,s^{-1}}$. Using this and Eqs. (B1)–(B9), the numerical values of surface acoustic wave mediated spin-spin interaction are given in Table II. We see that these values are comparable to or smaller than the contributions from bulk phonon-mediated spin-spin interaction. Note that the lower symmetry at the surface gives rise to terms that are odd in the orientation of the spins.

IV. CONCLUSION

In conclusion, we theoretically established a method to calculate the phonon-mediated spin-spin interaction in lattices. We first showed that the phonon-mediated spin-spin interaction cannot be determined properly in the Debye approximation, as unphysical distance-dependent oscillations appear. Next, we employed a fcc lattice to properly account for the Brillouin zone boundary and periodicity, where we showed that all phonon-mediated spin-spin interactions have a distance dependence of r^{-3}. We also estimated the phonon-mediated spin-spin interaction coupling in diamond NV centers and gave the energy level scheme of two interacting spin-1 systems, where we showed that the magnetic dipole-dipole interaction and phonon-mediated spin-spin interaction lift the fourfold degeneracy. Out of the nine energy levels (of which three are twofold degenerate), we discussed that six break the continuous rotational symmetry around the z axis and show a 3θ dependence under an applied magnetic field due to the phonon-mediated spin-spin interaction. Finally, we considered the surface acoustic wave mediated spin-spin interaction and showed that it has a distance dependence of r^{-3}, similar to the bulk phonon-mediated spin-spin interaction. We believe that a detailed understanding of the effect of phonons on quantum spins is a crucial step

TABLE III. Character table and basis of point group C_{3v}. The quadratics of spin S and strain tensor $u_{ij} = \partial_i u_j$ are decomposed into the irreducible representations.

Irrep	E	$2C_3$	$3\sigma_v$	Basis	SS	u_{ij}
A_1	1	1	1	z	S^{z2}	$u_{zz}, u_{xx} + u_{yy}$
A_2	1	1	-1	$xy - yx$	$-$	$u_{xy} - u_{yx}$
E	2	-1	0	(x, y)	$(\{S^y, S^z\}, -\{S^x, S^z\}),$	$(u_{yz} + u_{zy}, -u_{xz} - u_{zx}), (u_{xy} + u_{yx}, u_{xx} - u_{yy}),$
					$(\{S^x, S^y\}, S^{x2} - S^{y2}),$	$(-u_{yz} + u_{zy}, -u_{zx} + u_{xz})$

forward in the pursuit of quantum spin based precision measurements and computation. Finally, we remark that phonons in diamond also propagate in lower-dimensional systems such as one-dimensional rods and two-dimensional sheets, where we expect long-range phonon-mediated spin-spin coupling that is dominant over magnetic dipole-dipole interaction.

APPENDIX A: SYMMETRY CONSIDERATION ON SPIN-PHONON COUPLING

In this Appendix, we confirm the validity of the Hamiltonians (2)–(9) and (24) through a symmetry analysis. We identify six independent quadratic terms $S_i S_j$ in the spin. One of these terms is the identity $\sum_i S^{i2} = S(S + 1)$. The remaining five terms are decomposed into $A_1 \oplus 2E$ irreducible representations of C_{3v}, as detailed in Table III. Similarly, the nine strain tensor components, $u_{ij} = \partial_i u_j$, are decomposed into $2A_1 \oplus A_2 \oplus 3E$ irreducible representations.

Now, let us find the invariant forms of spin-phonon coupling. Both $S^{z2} u_{zz}$ and $S^{z2}(u_{xx} + u_{yy})$ terms can appear in the Hamiltonian as they belong to the A_1 irreducible representation as S^{z2}. The A_1 irreducible representations also arise from $E \times E$, defined by two E irreducible representations,

$$\boldsymbol{Q}_1 = (\{S^y, S^z\}, -\{S^z, S^x\}), \tag{A1}$$

$$\boldsymbol{Q}_2 = (\{S^x, S^y\}, S^{x2} - S^{y2}), \tag{A2}$$

as introduced in the main text. The shear strains

$$\boldsymbol{q}_1 = \tfrac{1}{2}(u_{yz} + u_{zy}, -u_{xz} - u_{zx}), \tag{A3}$$

$$\boldsymbol{q}_2 = \tfrac{1}{2}(u_{xy} + u_{yx}, u_{xx} - u_{yy}) \tag{A4}$$

and rotation

$$\boldsymbol{\omega} = \tfrac{1}{2}(u_{xz} - u_{zx}, u_{yz} - u_{zy}) \tag{A5}$$

share the same irreducible representation E as $\boldsymbol{Q}_i$, making their inner products with $\boldsymbol{Q}_i$, $\boldsymbol{Q}_i \cdot \boldsymbol{q}_j$ and $\boldsymbol{Q}_i \cdot \boldsymbol{\omega}$, totally symmetric in the C_{3v} point group and eligible for the Hamiltonian.

We should point out that $\tilde{q}_\parallel$ and $\tilde{q}_\perp$ ($\tilde{\boldsymbol{q}}_i$ and $\tilde{\boldsymbol{\omega}}$) in the main text belong to the A_1 (E) irreducible representation. Furthermore, upon taking the continuum limit, we find that they are in agreement with the above formulas:

$$\lim_{a \to 0} \tilde{q}_\parallel = u_{zz}, \tag{A6}$$

$$\lim_{a \to 0} \tilde{q}_\perp = u_{xx} + u_{yy}, \tag{A7}$$

$$\lim_{a \to 0} \tilde{\boldsymbol{q}}_1 = \tfrac{1}{2}(u_{yz} + u_{zy}, -u_{xz} - u_{zx}) = \boldsymbol{q}_1, \tag{A8}$$

$$\lim_{a \to 0} \tilde{\boldsymbol{q}}_2 = \tfrac{1}{2}(u_{xy} + u_{yx}, u_{xx} - u_{yy}) = \boldsymbol{q}_2, \tag{A9}$$

$$\lim_{a \to 0} \tilde{\boldsymbol{\omega}} = \tfrac{1}{2}(-u_{yz} + u_{zy}, -u_{xz} - u_{zx}) = \boldsymbol{\omega}, \tag{A10}$$

which are derived using Eq. (10). This confirms that $S^{z2}\tilde{q}_\parallel$, $S^{z2}\tilde{q}_\perp$, $\boldsymbol{Q}_i \cdot \tilde{\boldsymbol{q}}_j$, and $\boldsymbol{Q}_i \cdot \tilde{\boldsymbol{\omega}}$ are totally symmetric and can be included in the Hamiltonian.

APPENDIX B: SURFACE ACOUSTIC WAVE MEDIATED SPIN-SPIN INTERACTION COEFFICIENTS

In this Appendix, we give the surface acoustic wave mediated spin-spin interaction coefficients in Eq. (48). The shallow limit is taken to be $|x| \ll |\boldsymbol{r}_1 - \boldsymbol{r}_2|$, and only terms to the zeroth order in x are evaluated.

$$J_{zz}(r_z) \to \frac{-1}{2\pi \rho K_\sigma} \frac{1}{r_z^3 v_R^2}(\gamma^2 - 1)\left[h_\parallel h_\perp 4\left(1 - 2\eta\gamma \frac{1}{1 + \eta^2}\right) + h_\perp^2 \left(\frac{-(3 + 3\eta^2 + \gamma^2 + \eta^2\gamma^2 - 8\gamma\eta)}{(1 + \eta^2)}\right)\right], \tag{B1}$$

$$J_{zQ_1^2}(r_z) \to \frac{-1}{4\pi \rho K_\sigma} \frac{1}{v_R^2} \frac{1}{r_z^3} \frac{1}{(1 + \eta^2)^2}\left\{\frac{h_{eg,12}}{2}[2h_\parallel(1 + \eta^2 - 2\eta\gamma)(1 + \eta^2 + \gamma^2 - 4\eta\gamma + \eta^2\gamma^2)\right.$$

$$- h_\perp(3 + 6\eta^2 + 3\eta^4 - 12\eta\gamma - 12\eta^3\gamma + 16\eta^2\gamma^2 - 4\eta\gamma^3 - 4\eta^3\gamma^3 + \gamma^4 + 2\eta^2\gamma^4 + \eta^4\gamma^4)]$$

$$\left. + 2D\gamma(1 - \eta^2)(1 + \eta^2 - 2\eta\gamma)\mathrm{sgn}(r_z)(h_\parallel - h_\perp)\right\}, \tag{B2}$$

$$J_{zQ_2^2}(r_z) \rightarrow \frac{1}{-4\pi\rho K_\sigma} \frac{1}{r_z^3 v_R^2} \frac{1}{(1+\eta^2)^2} \Big(h_\parallel h_{\mathrm{eg},22}(1+\eta^2-2\eta\gamma)(1+\eta^2-4\eta\gamma+\gamma^2+\eta^2\gamma^2)$$

$$- h_\perp \frac{h_{\mathrm{eg},22}}{2}(3+6\eta^2+3\eta^4-12\eta\gamma-12\eta^3\gamma+16\eta^2\gamma^2-4\eta\gamma^3-4\eta^3\gamma^3+\gamma^4+2\eta^2\gamma^4+\eta^4\gamma^4) \Big), \quad \text{(B3)}$$

$$J_{Q_1^2 Q_1^2}(r_z) \rightarrow \frac{1}{4\pi\rho K_\sigma r_z^3 v_R^2} \frac{1}{(1+\eta^2)^2} \Big[\frac{h_{\mathrm{eg},12}^2}{8}(1+\eta^2-4\eta\gamma+\gamma^2+\eta^2\gamma^2)(-3-3\eta^2+4\eta\gamma+\gamma^2+\eta^2\gamma^2)$$

$$+ 4D^2\gamma^2(1-\eta^2)^2 \Big], \quad \text{(B4)}$$

$$J_{Q_1^2 Q_2^2}(r_z) \rightarrow \frac{1}{4\pi\rho K_\sigma} \frac{1}{r_z^3 v_R^2} \frac{1}{(1+\eta^2)^2} \Big[\frac{h_{\mathrm{eg},12}h_{\mathrm{eg},22}}{8}(1+\eta^2-4\eta\gamma+\gamma^2+\eta^2\gamma^2)(-3-3\eta^2+4\eta\gamma+\gamma^2+\eta^2\gamma^2)$$

$$+ \mathrm{sgn}(r_z)D\gamma h_{\mathrm{eg},22}(1-\eta^2)(1+\eta^2-2\eta\gamma) \Big], \quad \text{(B5)}$$

$$J_{Q_2^2 Q_2^2}(r_z) \rightarrow \frac{1}{4\pi\rho K_\sigma} \frac{1}{r_z^3 v_R^2} \frac{h_{\mathrm{eg},22}^2}{8} \frac{(1+\eta^2-4\eta\gamma+\gamma^2+\eta^2\gamma^2)(-3-3\eta^2+4\eta\gamma+\gamma^2+\eta^2\gamma^2)}{(1+\eta^2)^2}, \quad \text{(B6)}$$

$$J_{Q_1^1 Q_1^1}(r_z) \rightarrow \frac{1}{4\pi\rho K_\sigma} \frac{1}{r_z^3 v_R^2} h_{\mathrm{eg},11}^2 \left(1 - \frac{2\eta\gamma}{1+\eta^2} \right)^2, \quad \text{(B7)}$$

$$J_{Q_1^1 Q_2^1}(r_z) \rightarrow \frac{1}{4\pi\rho K_\sigma} \frac{1}{r_z^3 v_R^2} h_{\mathrm{eg},11}h_{\mathrm{eg},21} \left(1 - \frac{2\eta\gamma}{1+\eta^2} \right)^2, \quad \text{(B8)}$$

$$J_{Q_2^1 Q_2^1}(r_z) \rightarrow \frac{1}{4\pi\rho K_\sigma} \frac{1}{r_z^3 v_R^2} h_{\mathrm{eg},21}^2 \left(1 - \frac{2\eta\gamma}{1+\eta^2} \right)^2. \quad \text{(B9)}$$

[1] K. Sugihara, Spin-spin interaction in the paramagnetic salts, J. Phys. Soc. Jpn. **14**, 1231 (1959).

[2] L. K. Aminov and B. I. Kochelaev, Spin-spin interaction via a phonon field in paramagnetic crystals, Sov. Phys. JETP **15**, 903 (1962).

[3] D. H. McMahon and R. H. Silsbee, Virtual phonon effects in the paramagnetic resonance of MgO: Fe^{++}, Phys. Rev. **135**, A91 (1964).

[4] R. Orbach and M. Tachiki, Phonon-induced ion-ion coupling in paramagnetic salts, Phys. Rev. **158**, 524 (1967).

[5] J. Baker and A. Mau, EPR spectra of pairs of interacting rare-earth ions, Can. J. Phys. **45**, 403 (1967).

[6] J. Baker, Interactions between ions with orbital angular momentum in insulators, Rep. Prog. Phys. **34**, 109 (1971).

[7] A. Gruber, A. Dräbenstedt, C. Tietz, L. Fleury, J. Wrachtrup, and C. von Borczyskowski, Scanning confocal optical microscopy and magnetic resonance on single defect centers, Science **276**, 2012 (1997).

[8] J. F. Barry, J. M. Schloss, E. Bauch, M. J. Turner, C. A. Hart, L. M. Pham, and R. L. Walsworth, Sensitivity optimization for NV-diamond magnetometry, Rev. Mod. Phys. **92**, 015004 (2020).

[9] F. Jelezko, T. Gaebel, I. Popa, A. Gruber, and J. Wrachtrup, Observation of coherent oscillations in a single electron spin, Phys. Rev. Lett. **92**, 076401 (2004).

[10] J. Wrachtrup and F. Jelezko, Processing quantum information in diamond, J. Phys.: Condens. Matter **18**, S807 (2006).

[11] S. Pezzagna and J. Meijer, Quantum computer based on color centers in diamond, Appl. Phys. Rev. **8**, 011308 (2021).

[12] N. Y. Yao, L. Jiang, A. V. Gorshkov, P. C. Maurer, G. Giedke, J. I. Cirac, and M. D. Lukin, Scalable architecture for a room temperature solid-state quantum information processor, Nat. Commun. **3**, 800 (2012).

[13] M. Fukami, D. R. Candido, D. D. Awschalom, and M. E. Flatté, Opportunities for long-range magnon-mediated entanglement of spin qubits via on- and off-resonant coupling, PRX Quantum **2**, 040314 (2021).

[14] M. Fukami, J. C. Marcks, D. R. Candido, L. R. Weiss, B. Soloway, S. E. Sullivan, N. Delegan, F. J. Heremans, M. E. Flatté, and D. D. Awschalom, Magnon-mediated qubit coupling determined via dissipation measurements Proc. Natl. Acad. Sci. USA **121**, e2313754120 (2024).

[15] P. Udvarhelyi, V. O. Shkolnikov, A. Gali, G. Burkard, and A. Pályi, Spin-strain interaction in nitrogen-vacancy centers in diamond, Phys. Rev. B **98**, 075201 (2018).

[16] S. J. Whiteley *et al.*, Spin–phonon interactions in silicon carbide addressed by Gaussian acoustics, Nat. Phys. **15**, 490 (2019).

[17] S. Maekawa and M. Tachiki, Surface acoustic attenuation due to surface spin wave in ferro-and antiferromagnets, in *Magnetism and Magnetic Materials-1975*, AIP Conf. Proc. No. 29 (AIP, Melville, NY, 1976), pp. 542–543.

[18] The symmetry of the spin from a NV center, which is in the low-energy regime, is enhanced to D_{3d} with the addition of the spatial-inversion symmetry.

[19] J. J. Nakane and H. Kohno, Angular momentum of phonons and its application to single-spin relaxation, Phys. Rev. B **97**, 174403 (2018).

[20] The coupling with rotational deformation stems from the magnetic anisotropy Hamiltonian because the deformations of the form ε_{ij-} can also be regarded as the rotation of the global lattice from the perspective of the spin. Since only the C_∞ anisotropy $D(S^z)^2$ is considered in diamond NV centers, D_2 will not be considered.

[21] S.-F. Wang, Y.-F. Hsu, J.-C. Pu, J. C. Sung, and L. Hwa, Determination of acoustic wave velocities and elastic properties for diamond and other hard materials, Mater. Chem. Phys. **85**, 432 (2004).

[22] N. W. Ashcroft and N. D. Mermin, *Solid State Physics* (Thomson Learning Inc., 1976).

[23] K. Yoshida and H. Morigami, Thermal properties of diamond/copper composite material, Microelectron. Reliab. **44**, 303 (2004).

[24] A. M. Kosevich, *The Crystal Lattice: Phonons, Solitons, Dislocations, Superlattices* (Wiley-VCH, Berlin, 2006).

[25] A. F. Andreev and Yu. A. Kosevich, Capillary phenomena in the theory of elasticity, Sov. Phys. JETP **54**, 761 (1981).

[26] T. Staudacher, F. Shi, S. Pezzagna, J. Meijer, J. Du, C. A. Meriles, F. Reinhard, and J. Wrachtrup, Nuclear magnetic resonance spectroscopy on a (5-nanometer)^3 sample volume, Science **339**, 561 (2013).

[27] M. Loretz, S. Pezzagna, J. Meijer, and C. L. Degen, Nanoscale nuclear magnetic resonance with a 1.9-nm-deep nitrogen-vacancy sensor, Appl. Phys. Lett. **104**, 033102 (2014).

[28] C. Müller *et al.*, Nuclear magnetic resonance spectroscopy with single spin sensitivity, Nat. Commun. **5**, 4703 (2014).

[29] H. Ezawa, Phonons in a half space, Ann. Phys. (NY) **67**, 438 (1971).

[30] L. D. Landau and E. M. Lifshitz, *Theory of Elasticity*, 3rd ed. (Pergamon, Oxford, 1986).

[31] M. Mohr, A. Caron, P. Herbeck-Engel, R. Bennewitz, P. Gluche, K. Brühne, and H.-J. Fecht, Young's modulus, fracture strength, and Poisson's ratio of nanocrystalline diamond films, J. Appl. Phys. **116**, 124308 (2014).